after 5 min of digestion. Three of the serum samples also reacted with FR 2, FR 3, and FR 4 after 30 min of digestion.

The three samples that react with FR 2, FR 3, and FR 4 were obtained from patients who exhibited persistent allergies to egg white. One of these serum samples, No.4, was obtained from a 3-year-old girl who is presently 6 years old; her total IgE level has decreased slightly to 4,450 IU/ml, but the specific IgE level for egg white remains at more than 100 IU/ml, and the patient has not outgrown her hypersensitivity to eggs. Another patient, No. 13, was a 1-year-old boy; 7 years later, his total and egg white-specific IgE levels had been reduced to 947 and 6.85 IU/ml, respectively, but eating raw eggs still caused allergic symptoms. The third FR 4-positive patient, No. 19, was an 11-year-old boy whose total IgE level decreased to 3,940 IU/ml and whose egg white-specific IgE decreased to 13.5 IU/ml after a period of about 2 years; however, this patient has also not outgrown his allergies. These cases and our previously reported data [17] indicate that the induction of egg white tolerance may be difficult in patients whose serum IgE exhibits binding activity to digested small fragments of OVM.

Discussion

In the SGF-digestion system, preheating the OVM (100°C for 5 or 30 min) did not affect the OVM digestion pattern (fig. 1), consistent with the results of previous reports [9] in which heat treatment did not markedly decrease the allergenicity of OVM. On the other hand, a decrease in the pepsin/OVM ratio dramatically reduced the digestion rate, suggesting that digestibility may vary depending on the amount of OVM intake and the conditions of the individual's digestion system. In its native state, OVM possesses serine protease inhibitor activity. Fu et al. [11] and our group [10] previously reported that intact OVM was stable for 60 min in simulated intestinal fluid. Kovacs-Nolan et al. [15] also reported that pepsin-

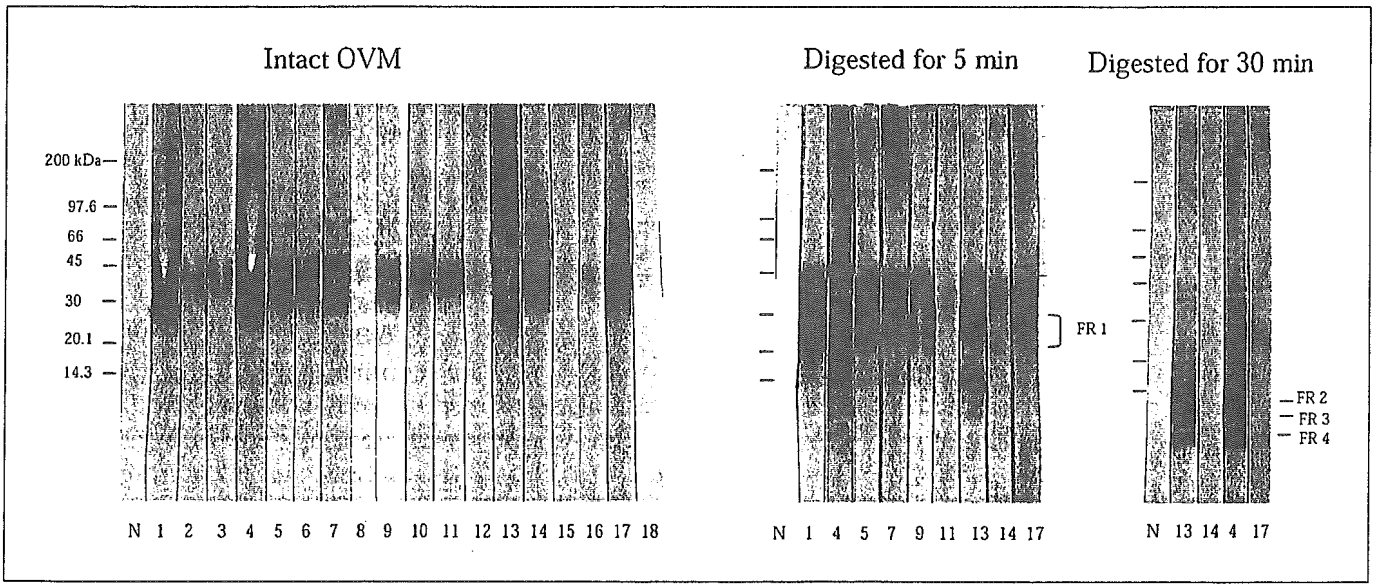

Fig. 4. Amino acid sequence and schematic representation of the SGF-digestion pattern of OVM. The amino acid sequence of OVM is shown in the upper panel. The arrows indicate the SGF-digested points according to the results of an N-terminal analysis of the OVM fragments (table 1), and the underlined regions indicate sequences identified by LC/MS/MS. Solid line = FR 1; dotted line = FR 3; dashed line = FR 4. Shaded areas represent reported human IgE epitopes [16]. The lower panel is a summary of the OVM digestion pattern according to N-terminal analysis.

Fig. 5. Western blot analysis of intact OVM and the fragments with serum IgE from egg white allergic patients and a normal volunteer. The fragments were prepared as described in the legend of figure 2. The number of each strip corresponds to the sample numbers in table 2.

Table 3. Reactivity of OVM and pepsin fragments with patient serum IgE

No.	IgE content, IU/ml		Reactivity with patient IgE[1]				
	total	egg white-specific	intact OVM	FR 1	FR 2	FR 3	FR 4
1	3,700	>100	+++	++	–	–	–
2	402	3.74	+	n.d.	n.d.	n.d.	n.d.
3	251	6.85	+	n.d.	n.d.	n.d.	n.d.
4	6,510	>100	+++	+++	+	+	++
5	2,060	>100	++	++	–	–	–
6	1,240	12.4	++	n.d.	n.d.	n.d.	n.d.
7	4,180	31.3	++	++	–	–	–
8	56	20.1	±	n.d.	n.d.	n.d.	n.d.
9	1,355	50.7	++	++	–	–	–
10	22,810	2.11	+	n.d.	n.d.	n.d.	n.d.
11	1,463	4.65	+	–	–	–	–
12	14,230	0.70–3.49	±	n.d.	n.d.	n.d.	n.d.
13	8,000	>100	+++	+++	+	+	++
14	22,490	1.05	+++	±	–	–	–
15	934	66.3	+	n.d.	n.d.	n.d.	n.d.
16	345	20.1	+	n.d.	n.d.	n.d.	n.d.
17	1,500	80	++	+	–	–	–
18	3,300	>10	–	n.d.	n.d.	n.d.	n.d.
19	20,500	26.8	+++	++	±	±	±
20	138	45.4	++	+	–	–	–
21	940	2.44	+	+	–	–	–
22	91	0.70–3.49	+	±	–	–	–
23	828	0.9	++	+	–	–	–
24	21	3.50–17.4	–	n.d.	n.d.	n.d.	n.d.
	positive/tested		22/24 (92%)[2]	13/14 (93%)[3]	3/14 (21%)[3]	3/14 (21%)[3]	3/14 (21%)[3]

n.d. = Not done.

[1] Intensity of the reactivity of each band was evaluated by the ratio to normal serum: – = <1; ± = 1–2; + = 2–5; ++ = 5–10; +++ = >10.

[2] Percent of egg white-positive samples.

[3] Percent of intact OVM-positive samples.

digested OVM retains its trypsin inhibitor activity. Therefore, OVM and its pepsin-digested fragments were thought to be stable in the small intestine.

At a pepsin/OVM ratio of 1 unit/μg, FR 1 reached a maximum level after 2 min of digestion, while both FR 2 and FR 3 reached maximum levels after 5 min of digestion; thereafter, FR 1, FR 2, and FR 3 gradually decreased. However, FR 4 increased continuously throughout the 30-min period of digestion and the major fragments were seen after 30 min of digestion (fig. 3). FR 4 was mainly composed of three fragments whose N-terminals were 134V, 104N and 19V (table 1). A C-terminal sequence, 165N–185C, was also identified in FR 4 (table 2). These fragments contain known IgE epitopes [19] and therefore may cause allergic responses. Three of the OVM-positive sera from patients with egg white allergy reacted positively with the FR 4 fragments (table 3).

The present results are consistent with the previous finding that pediatric subjects with a higher IgE-binding activity to pepsin-treated OVM were unlikely to outgrow their egg allergy [17]. For peanut allergies, differences in IgE-binding epitopes have been reported between the patients with clinically active peanut allergies and those who developed a tolerance, regardless of the presence of high or low peanut-specific IgE levels [20].

The N-terminal residue of the major fragment (4-1) of FR 4 was Val-134 (30%; table 1). This fragment retains most of domain III, which has been reported to have significantly higher human IgG- and IgE-binding activities than those of domains I and II [12]. A domain-III OVM

variant has also been reported to cause a reduction in immunogenicity and allergenicity [21].

Domains I, II, and III contain one, three, and one N-glycosylation sites, respectively [7]. The possible relation between the carbohydrate chain in domain III and allergenicity is interesting. One report suggested that this carbohydrate chain may play an important role in allergenic determinants against human IgE antibody [13], and another report suggested that the carbohydrate chains of OVM may protect against peptic hydrolysis [22]. However, the carbohydrate moieties have been shown to have only a minor effect on allergenicity [23]. As shown in figure 2, intact OVM, FR 1, and FR 2 fragments were detected using PAS staining, suggesting the presence of carbohydrate chains, but FR 4 was not stained with the PAS reagent, despite being clearly detected with CBB. Therefore, FR 4 might contain little or no carbohydrate chains. Since FR 4 seems to maintain its allergenic potential, as described above, the absence of the carbohydrate chains in FR 4 suggests that they are not necessary for OVM allergenicity. Since the minimum peptide size capable of eliciting significant clinical symptoms of allergic reactions is thought to be 3.1 kDa [24], FR 4 may be able to trigger mast cell activation and elicit clinical symptoms.

In this report, the SGF-digestion kinetic pattern of OVM was investigated in detail, and the partial sequences of the fragments in the 4 fractions separated by SDS-PAGE were determined. Furthermore, the reactivity of the fragments with a number of serum samples from patients with egg white allergies was detected using Western blotting. The four fractions were separated according to their molecular weight and consisted of more than one fragment, as determined by N-terminal analysis. The identified sequences that started at Asn-104 and Val-134 in FR 3, as determined using LC/MS/MS (table 2), coincided with the 3-2 and 3-3 fragments in the N-terminal analysis (table 1), and the sequence that started at Asn-104 in FR 4 coincided with fragment 4-2. Moreover, the LC/MS/MS analysis indicated that FR 3 and FR 4 contained other parts of domain II and the C-terminal sequence N165–C185, which are thought to be minor components of these fractions. The combination of SGF digestion and patient IgE may provide useful information for the diagnosis and prediction of potential OVM allergenicity.

Acknowledgement

This study was supported by a grant from the Ministry of Health, Labor and Welfare, and the Cooperative System for Supporting Priority Research of Japan Science and Technology Agency.

References

1 Sampson HA, McCaskill CC: Food hypersensitivity and atopic dermatitis: Evaluation of 113 patients. J Pediatr 1985;107:669–675.
2 Bock SA, Sampson HA, Atkins FM, Zeiger RS, Lehrer S, Sachs M, Bush RK, Metcalfe DD: Double-blind, placebo-controlled food challenge (DBPCFC) as an office procedure: A manual. J Allergy Clin Immunol 1988;82:986–997.
3 Bock SA, Atkins FM: Patterns of food hypersensitivity during sixteen years of double-blind, placebo-controlled food challenges. J Pediatr 1990;117:561–567.
4 Boyano-Martinez T, Garcia-Ara C, Diaz-Pena JM, Martin-Esteban M: Prediction of tolerance on the basis of quantification of egg white-specific IgE antibodies in children with egg allergy. J Allergy Clin Immunol 2002;110:304–309.
5 Kotaniemi-Syrjanen A, Reijonen TM, Romppanen J, Korhonen K, Savolainen K, Korppi M: Allergen-specific immunoglobulin E antibodies in wheezing infants: The risk for asthma in later childhood. Pediatrics 2003;111:e255–e261.
6 Li-Chan E, Nakai S: Biochemical basis for the properties of egg white. Crit Rev Poultry Biol 1989;2:21–58.
7 Kato I, Schrode J, William J. Kohr WJ, Laskowski M Jr: Chicken ovomucoid: Determination of its amino acid sequence, determination of the trypsin reactive site, and preparation of all three of its domains. Biochemistry 1987;26:193–201.
8 Matsuda T, Watanabe K, Nakamura R: Immunochemical and physical properties of peptic-digested ovomucoid. J Agric Food Chem 1983;31:942–946.
9 Honma K, Aoyagi M, Saito K, Nishimuta T, Sugimoto K, Tsunoo H, Niimi H, Kohno Y: Antigenic determinants on ovalbumin and ovomucoid: Comparison of the specificity of IgG and IgE antibodies. Arerugi 1991;40:1167–1175.
10 Takagi K, Teshima R, Okunuki H, Sawada J: Comparative study of in vitro digestibility of food proteins and effect of preheating on the digestion. Biol Pharm Bull 2003;26:969–973.
11 Fu TJ, Abbott UR, Hatzos C: Digestibility of food allergens and nonallergenic proteins in simulated gastric fluid and simulated intestinal fluid-a comparative study. J Agric Food Chem 2002;50:7154–7160.
12 Zhang JW, Mine Y: Characterization of IgE and IgG epitopes on ovomucoid using egg-white-allergic patients' sera. Biochem Biophys Res Commun 1998;253:124–127.
13 Matsuda T, Nakamura R, Nakashima I, Hasegawa Y, Shimokata K: Human IgE antibody to the carbohydrate-containing third domain of chicken ovomucoid. Biochem Biophys Res Commun 1985;129:505–510.
14 Thomas K, Aalbers M, Bannon GA, Bartels M, Dearman RJ, Esdaile DJ, Fu TJ, Glatt CM, Hadfield N, Hatzos C, Hefle SL, Heylings JR, Goodman RE, Henry B, Herouet C, Holsapple M, Ladics GS, Landry TD, MacIntosh SC, Rice EA, Privalle LS, Steiner HY, Teshima R, Van Ree R, Woolhiser M, Zawodny J: A multi-laboratory evaluation of a common in vitro pepsin digestion assay protocol used in assessing the safety of novel proteins. Regul Toxicol Pharmacol 2004;39:87–98.

15 Kovacs-Nolan J, Zhang JW, Hayakawa S, Mine Y: Immunochemical and structural analysis of pepsin-digested egg white ovomucoid. J Agric Food Chem 2000;48:6261–6266.
16 Besler M, Petersen A, Steinhart H, Paschke A: Identification of IgE-Binding Peptides Derived from Chemical and Enzymatic Cleavage of Ovomucoid (Gal d 1). Internet Symposium on Food Allergens 1999;1:1–12. http://www.food-allergens.de
17 Urisu A, Yamada K, Tokuda R, Ando H, Wada E, Kondo Y, Morita Y: Clinical significance of IgE-binding activity to enzymatic digests of ovomucoid in the diagnosis and the prediction of the outgrowing of egg white hypersensitivity. Int Arch Allergy Immunol 1999; 120:192–198.
18 Zacharius RM, Zell TE, Morrison JH, Woodlock JJ: Glycoprotein staining following electrophoresis on acrylamide gels. Anal Biochem 1969;30:148–152.
19 Mine Y, Zhang JW: Identification and fine mapping of IgG and IgE epitopes in ovomucoid. Biochem Biophys Res Commun 2002; 292:1070–1074.
20 Beyer K, Ellman-Grunther L, Jarvinen KM, Wood RA, Hourihane J, Sampson HA: Measurement of peptide-specific IgE as an additional tool in identifying patients with clinical reactivity to peanuts. J Allergy Clin Immunol 2003;112:202–207.
21 Mine Y, Sasaki E, Zhang JW: Reduction of antigenicity and allergenicity of genetically modified egg white allergen, ovomucoid third domain. Biochem Biophys Res Commun 2003; 302:133–137.
22 Matsuda T, Gu J, Tsuruta K, Nakamura R: Immunoreactive glycopeptides separated from peptic hydrolysate of chicken egg white ovomucoid. J Food Sci 1985;50:592–594.
23 Cooke SK, Sampson HA: Allergenic properties of ovomucoid in man. J Immunol 1997;159: 2026–2032.
24 Kane PM, Holowka D, Baird B: Cross-linking of IgE receptor complexes by rigid bivalent antigens greater than 200 Å in length triggers cellular degranulation. J Cell Biol 1988;107: 969–980.

Expression of Annexin A3 in Primary Cultured Parenchymal Rat Hepatocytes and Inhibition of DNA Synthesis by Suppression of Annexin A3 Expression Using RNA Interference

Shingo NIIMI,*[a] Mizuho HARASHIMA,[b] Masaru GAMOU,[b] Masashi HYUGA,[a] Taiichiro SEKI,[b] Toyohiko ARIGA,[b] Toru KAWANISHI,[a] and Takao HAYAKAWA[c]

[a] *Division of Biological Chemistry and Biologicals, National Institute of Health Sciences; 1–18–1 Kamiyoga, Setagaya-ku, Tokyo 158–8501, Japan:* [b] *Department of Nutrition and Physiology, Nihon University College of Bioresource Sciences; Kameino, Fujisawa 252–8510, Japan; and* [c] *Deputy Director General, National Institute of Health Sciences; 1–18–1 Kamiyoga, Setagaya-ku, Tokyo 158–8501, Japan.*

Received October 30, 2004; accepted January 5, 2005; published online January 7, 2005

Annexin A3 is a member of the lipocortin/annexin family, which binds to phospholipids and membranes in a Ca^{2+}-dependent manner. Although annexin A3 has various functions *in vitro*, its cellular significance is completely unknown. Annexin A3 is not found in rat liver *in vivo*. In the present study, we investigated the expression of annexin A3 in primary cultured parenchymal rat hepatocytes. Annexin A3 protein was detected in 48-h, but not 2.5-h, cultured hepatocytes using Western blot analysis. The annexin A3 level further increased after an additional 24 h of culture. Annexin A3 mRNA was not detected in 2.5-h cultured hepatocytes but was detected 22 h after the start of culture by RT-PCR analysis, reaching a maximum value after 48 h of culture. To define the role of Annexin A3 in DNA synthesis, RNA interference was used to reduce annexin III gene expression in hepatocytes. The transfection of small interfering RNAs targeting annexin A3 in the hepatocytes reduced the corresponding mRNA and protein expression by approximately 80% and more than 90%, respectively, at 24 h after transfection. In the annexin A3 small interfering RNAs-transfected cells, DNA synthesis, as assessed by [^{3}H]thymidine incorporation, decreased by approximately 70% not only in the control cultures, but also in the hepatocyte growth factor- or epidermal growth factor-treated cells. These findings show that annexin A3 is expressed in primary cultured parenchymal rat hepatocytes and that the suppression of annexin A3 expression using RNA interference inhibits DNA synthesis.

Key words annexin A3; RNAi; DNA synthesis; primary cultured hepatocyte; hepatocyte growth factor (HGF); epidermal growth factor (EGF)

Annexin (Anx) A3 is also called "lipocortin 3" or "placental anticoagulant protein 3" (PAP-III)[1] and is a member of the lipocortin/annexin family, which binds to phospholipids and membranes in a Ca^{2+}-dependent manner.[2—4] AnxA3 has been shown to have anticoagulant and anti-phospholipase A_2 properties *in vitro*[5] and to promote the Ca^{2+}-dependent aggregation of isolated specific granules from human neutrophils.[6] Although the physiological functions of other annexins have been recently clarified in knock-out and transgenic models,[7—14] the functions of AnxA3 are completely unknown.[15]

Recently, we found that AnxA3 protein and its mRNA are not expressed in isolated parenchymal rat hepatocytes.[16,17] Consistent with these findings, AnxA3 protein and its mRNA are not detectable by Western blot analysis and Northern blot analysis in rat liver.[18—21] However, there have been no reports on the behavior of AnxA3 in primary cultured parenchymal rat hepatocytes. In the present study, we investigated the expression and function of AnxA3 in cultured parenchymal rat hepatocytes.

MATERIALS AND METHODS

Materials Recombinant human hepatocyte growth factor (HGF) was purchased from R&D systems (Minneapolis, MN, U.S.A.). Mouse epidermal growth factor (EGF) was purchased from Wako (Osaka, Japan). [^{3}H]thymidine (79.9 Ci/mmol) was purchased from PerkinElmer (Boston, MA, U.S.A.). Rabbit anti-human ANXA3 antibody serum was a generous gift from Dr. F. Russo-Marie and Dr. C. Raguenness-Nicol.

Cell Isolation and Monolayer Cultures Parenchymal hepatocytes were isolated from adult male Wistar rats, weighing 180—200 g, by *in situ* perfusion of the liver with collagenase.[22] All animal care and procedure protocols were approved by the institutional care committee. The cells were then suspended at a density of 2.5×10^5 cells/ml in Williams E medium (WE) containing 5% fetal bovine serum and 1 nM insulin and cultured at a density of 0.5×10^5 cells/cm^2 in a 6 cm dish and a 48-well microplate precoated with collagen type-1 AC in a humidified chamber at 37 °C in 5% CO_2 and 30% O_2 in air. Cells plated in the 6-cm dish and 48-well microplate were used to prepare total cellular extracts or total RNA and to measure DNA synthesis, respectively. After 2.5 h of culture, the medium was replaced with a serum- and hormone-free medium containing aprotinin (1 μg/ml).

Western Blot Analysis Cell lysates were prepared using a modification of a previously described method.[23] The cells were washed with phosphate-buffered saline (PBS) followed by buffer A (50 mM Tris–HCl [pH 7.5], 150 mM NaCl, and 10 mM EDTA). The cells were then harvested after the addition of 20 μl of buffer A. The cells were suspended, shaken for 15 min at room temperature, and sonicated five times for 15 s each time while in an ice bath after the addition of 1/5 [v/v] of 5×buffer A containing 2.5% Triton X-100 and 1/100 [v/v] of a protease inhibitor cocktail (SIGMA). After centrifugation at $100000\times g$, the cytosolic fraction (about 25 μg) was subjected to sodium dodecyl sulfate-polyacrylamide gel

* To whom correspondence should be addressed. e-mail: niimi@nihs.go.jp

electrophoresis on a 10% gel and electroblotted to a PVDF membrane (GVHP; Millipore). After blocking the membrane with 5% skimmed milk, a Western blot analysis was performed using rabbit anti-human AnxA3 antibody serum at a dilution of 1 : 18000; detection was performed using the ECL detection system (Amersham Bioscience).

Reverse Transcription Polymerase Chain Reaction Analysis Total RNA was exctracted from the cells using Trizol reagent (Invitrogen) according to the manufacturer's protocols. Approximately 3 μg of RNA per sample was reverse-transcribed using the THERMOSCRIPT™ RT-PCR System (Invitrogen) and oligo$(dT)_{20}$ in a final volume of 40 μl, according to the manufacturer's protocols. Subsequently, 1 μl of cDNA was polymerase chain reaction (PCR)-amplified using the THERMOSCRIPT™ RT-PCR System (Invitrogen) in a final volume of 20 μl per reaction, according to the manufacturer's protocols, for 14—23 cycles of denaturation for 30 s at 94 °C, annealing for 30 s at 60 °C, and polymerization for 1 min at 72 °C using Anx AIII or glyceraldehyde 3-phosphate dehydrogenase (GAPDH) cDNA specific primers under linear conditions. The PCR products were separated on a 2% agarose gel, stained with SYBR Green I, and visualized and analyzed with a FluorolImager 595 (Amersham Bioscience). A computer assisted-analyzer was used to quantitatively analyze the signals, and the signals were normalized to the signal of a house keeping gene, the gene coding GAPDH. The sequences of the AnxA3 primers were as follows: 5′-CAAATTCACCGAGATCCTGT-3′ and 5′-TGCTGGAGTGCTGTACGAAA-3′. The sequences of the GAPDH primers were as follows: 5′-ACCACAGTCCATGCCATCAC-3′ and 5′-TCCACCACCTGTTGCTGTA-3′.[24] The PCR product specificity was confirmed by DNA sequence analysis using an ABI Prism 377 DNA Sequencer (Applied Biosystems, Foster City, CA, U.S.A.).

Preparation and Transfection of Small Interfering RNAs Targeting AnxA3 Small interfering RNAs (siRNAs) targeting rat AnxA3 were designed according to the guidelines of the "Dharmacon siDESIGN Center" (www.dharmacon.com) and obtained from Dharmacon Research (Lafayette) in annealed and lyophilized forms. The target sequences were localized at positions, 493 and 690 bps downstream of the start codon. The sequences of each siRNA pair were as follows: AnxA3 siRNA 1, 5′-GAG ACG AAA GCC UGA AAG UdTdT-3′ and ACU UUC AGG CUU UCG UCU cdTdT-3′; ANXA3 siRNA 2, 5′-GGA GAA UUA UCU GGG CAU UdTdT-3′ and AAU GCC CAG AUA AUUCUC cdTdT-3; and control siRNA, 5′-ACU CUA UCU GCA CGC UGA CUU-3′ and 5′-P G UCA GCG UGC AGA UAG AGU UU-3′. No homology between any relevant mammalian gene and the control siRNA was observed. These siRNAs were dissolved in an RNase-free solution provided by Dharmacon Research at a concentration of 20 μM. After 20 h of cell culture, the medium was replaced with WE containing aprotinin (1 μg/ml) immediately prior to transfection. Transfection with siRNA was performed using SiFector (B-bridge), according to the user guidelines. Sixty microliters of both AnxA3 siRNA 1 and 2 were diluted with OPTI-MEM (Invitrogen) to a final volume of 400 μl. Sixty-four microliters of SiFector was also diluted in OPTI-MEM to a final volume of 400 μl, then suspended and incubated at room temperature for 5 min. Next, the diluted siRNA was combined with SiFector, and the mixture was incubated at room temperature to allow the siRNA-SiFector complex to form. Eight hundred microliters of the siRNA-SiFector complex was added to the cultures (6-cm dish). For the 48-well plates, the siRNA-SiFector complex was prepared as described above except that the volume of each solution per well was scaled down to 1/16.

Measurement of [^{3}H]thymidine Incorporation After 20 h of culture, the medium was replaced with hormone-free medium containing aprotinin (1 μg/ml) and 0.1% bovine serum albumin (BSA), and EGF (2 ng/ml) or HGF (20 ng/ml) was added. After 1 h, 50 μl of siRNA-SiFector complex, prepared as described above, was added to the wells. After another 24 h, [^{3}H]thymidine (0.626 μCi) and thymidine (676.6 ng) were added, and 10 μg/ml of aphidicolin was added to some wells at the same time. The cells were then cultured for another 24 h. [^{3}H]thymidine incorporation was measured as described previously.[25] The difference between the radioactivity in the hot-trichloroacetic acid soluble fraction with and without aphidicolin was calculated as dpm/mg protein. Cell protein was measured using a previously described method,[26] with BSA used as a standard.

RESULTS

Expression of AnxA3 during Culture At first, we investigated the expression of AnxA3 in primary cultured parenchymal rat hepatocytes. AnxA3 protein was not detected by Western blot analysis 2.5 and 24 h after the start of culture but was detected after 48 h of culture (Fig. 1A). The level after 72 h of culture was approximately 1.6-fold higher than that after 48 h of culture (Fig. 1B). AnxA3 mRNA was not detected by reverse transcription (RT)-PCR in cultured hepatocytes after 2.5 h of culture but was significantly detected after 22 h of culture (Fig. 2A), reaching a maximum value after 48 h of culture (Fig. 2B). These results indicate

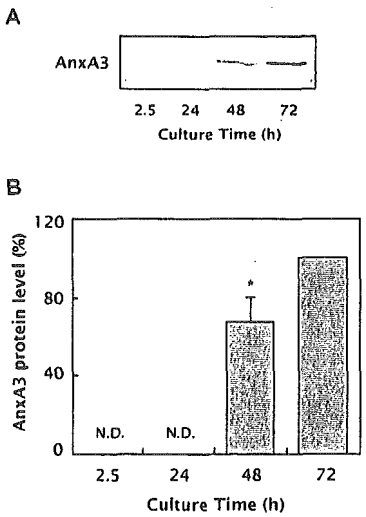

Fig. 1. Expression of AnxA3 Protein during Culture

(A) The data shown are representative of the Western blot analysis results. Cells lysates were prepared from the cells at the indicated times and used for the Western blot analysis. (B) The intensity of each band was quantified, and the results are shown relative to the value of cells cultured for 72 h. The data are expressed as the mean±S.D. of 3 experiments. *$p<0.01$, compared with the value of cells cultured for 72 h. N.D., not detected.

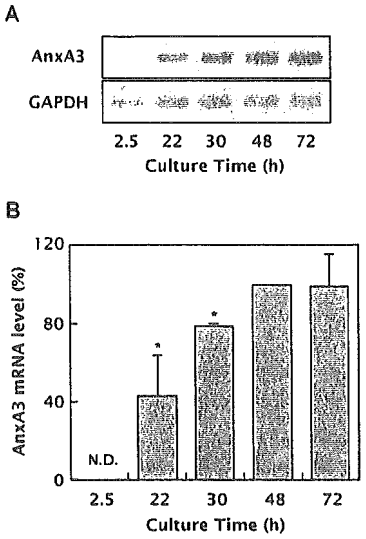

Fig. 2. Increase in AnxA3 mRNA Level during Culture

(A) The data shown are representative of the RT-PCR analysis results. Total RNA was prepared from the cells at the indicated times and used for the RT-PCR analysis. (B) The intensity of each band was quantified, and the results are shown relative to the value of cells cultured for 48 h. The data are expressed as the mean±S.D. of 3 experiments. *$p<0.01$, compared with the value of cells cultured for 48 h. N.D., not detected.

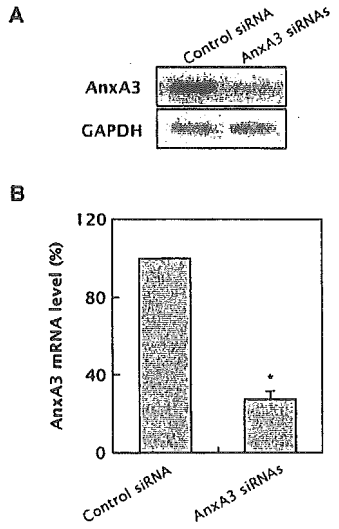

Fig. 3. Suppression of Increase in AnxA3 mRNA Level during Culture with RNAi

(A) The data shown are representative of the RT-PCR analysis results. Total RNA was prepared from the cells 1 d after siRNA transfection and used for the RT-PCR analysis. (B) The intensity of each band was quantified, and the results are shown relative to the value of cells transfected with control siRNA. The data are expressed as the mean±S.D. of 3 experiments. *$p<0.01$, compared with the value of cells transfected with control siRNA.

that the expression of AnxA3 is regulated by its mRNA level.

Suppression of AnxA3 Expression Using RNA Interference Next, we attempted to suppress AnxA3 expression by RNA interference (RNAi) to examine the role of ANXA3 in the cultured hepatocytes. AnxA3 mRNA expression was markedly reduced by treatment with AnxA3 siRNAs, compared with the expression after treatment with control siRNA, 1 d after the transfection (Fig. 3A), with an inhibition of approximately 80% (Fig. 3B). Furthermore, the AnxA3

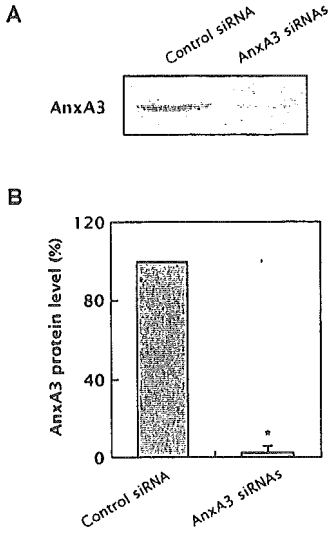

Fig. 4. Suppression of AnxA3 Protein Expression during Culture with RNAi

(A) The data shown are representative of the Western blot analysis results. Cells lysates were prepared from the cells 1 d after siRNA transfection and used for the Western blot analysis. (B) The intensity of each band was quantified, and the results are shown relative to the value of cells transfected with control siRNA. The data are expressed as the mean±S.D. of 3 experiments. *$p<0.01$, compared with the value of cells transfected with control siRNA.

protein level was also reduced by the treatment with AnxA3 siRNAs compared with the level after treatment with control siRNA (Fig. 4A), with an inhibition of more than 95% (Fig. 4B). On the other hand, the control siRNA had almost no effect on AnxA3 protein and mRNA levels compared with those treated with SiFector alone (data not shown). Neither the control nor AnxA3 siRNAs caused any cytotoxic effects, as observed microscopically or by the quantification of the total amount of protein in each sample (data not shown). These results indicate that AnxA3 siRNAs efficiently and specifically, inhibit the expression of AnxA3 in primary cultured parenchymal rat hepatocytes.

Inhibition of DNA Synthesis by Suppression of AnxA3 Expression Using RNAi Finally, we examined the role of AnxA3 in DNA synthesis by suppressing AnxA3 expression using RNAi. EGF (2 ng/ml) and HGF (20 ng/ml) stimulated DNA synthesis by approximately 7-fold and 9-fold, respectively in hepatocytes treated with control siRNA (Fig. 5). The stimulations were inhibited to approximately 70% by treatment with AnxA3 siRNAs. Similar results were also obtained in the control cells, whereas the control siRNA had almost no effect on DNA synthesis, compared with the effect in cells treated with SiFector alone (data not shown).

DISCUSSION

In the present study, we showed for the first time that AnxA3 is expressed in cultured parenchymal rat hepatocytes and that the inhibition of AnxA3 expression by RNAi resulted in a significant inhibition of DNA synthesis, suggesting that the expression of AnxA3 is necessary for DNA synthesis in primary cultured parenchymal rat hepatocytes.

Hepatocytes placed under culture conditions, are known to acquire a growth potential characterized by the enhancement of DNA synthesis, which is caused by several growth

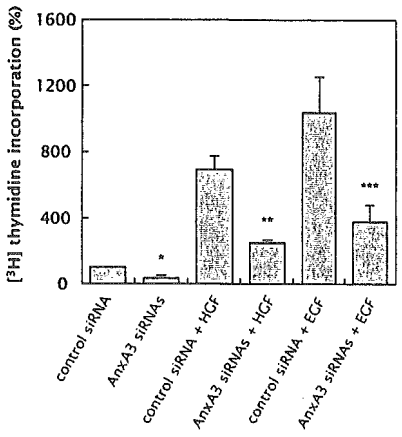

Fig. 5. Inhibition of DNA Synthesis by RNAi

The results are shown relative to the value of control cultured cells transfected with control siRNA. The data are expressed as the mean±S.D. of duplicate wells in 3 experiments. *$p<0.01$, compared with the value of control cultured cells transfected with control siRNA. **$p<0.01$, compared with the value of cells cultured in the presence of HGF and transfected with control siRNA. ***$p<0.01$, compared with the value of cells cultured in the presence of EGF and transfected with control siRNA. The mean±S.D. of [^{3}H]thymidine incorporation in the control cultured cells transfected with control siRNA was $9.72\times10^4\pm0.68\times10^4$ dpm/mg protein.

factors.[27,28] Our present findings suggest that the expression of AnxA3 is partly necessary for hepatocytes to acquire a growth potential under culture conditions. In fact, the enhanced expression of AnxA3 has been observed in hepatocellular carcinoma cell lines.[29] In addition, we discovered that the enhanced expression of Anx3 was observed in the proliferative hepatocytes after carbon tetrachloride-induced rat liver damage (unpublished observations).

As for other annexins, several findings concerning the relation of AnxA1 to hepatocyte growth has been reported as described below. The suppression of AnxA1 expression using antisense technology inhibited proliferation in a mouse hepatocyte cell line.[30] AnxA1 increased in the proliferative hepatocytes after carbon tetrachloride-induced rat liver damage or a partial hepatectomy and in hepatocellullar carcinoma tissue.[31,32]

Although the mechanism of action of AnxA3 on DNA synthesis is presently uncertain, the target of AnxA3 may be a common signal transduction pathway, and not necessarily a constitutive or growth factor-mediated one, because the suppression of AnxA3 expression using RNAi not only inhibited the control of DNA synthesis, but also EGF- or HGF-stimulated DNA synthesis, almost to a similar level. In this respect, the findings described below may be relevant to speculations on the mechanism of action of AnxA3 on DNA synthesis. The growth factor-mediated enhancement of hepatocyte growth consists of several signal transduction pathways.[33] The activation of cytosolic phospholipase A_2 ($cPLA_2$) by MAP kinase liberates arachidonic acid from phospholipids and is followed by the generation of prostaglandins, mediators of DNA synthesis, *via* cyclooxygenase. Interestingly, the suppression of AnxA1 expression using antisense technology inhibited $cPLA_2$ activity in a mouse hepatocyte cell line.[30] This report suggests that $cPLA_2$ must be phosphorylated by AnxA1 to become active. Additional evidence suggests that AnxA1 (275—346 aa), the region responsible for phospholipid binding is necessary for the interaction between AnxA1 and $cPLA_2$.[34] Further study is required to clarify the mechanism of action of AnxA3, including the possibility that AnxA3 positively modulates $cPLA_2$ activity, as in the case of AnxA1.

Acknowledgements This work was supported by grants for Health and Welfare Research from the Japanese Ministry of Health, Labor and Welfare.

REFERENCES

1) Crumpton M. J., Dedman J. R., *Nature* (London), **345**, 212 (1990).
2) Raynal P., Pollard H. B., *Biochim. Biophys. Acta*, **1197**, 63—93 (1994).
3) Gerke V., Moss S. E., *Physiol. Rev.*, **82**, 331—371 (2002).
4) Moss S. E., Morgan R. O., *Genome Biol.*, **5**, 219. 1—8 (2004).
5) Tait J. F., Sakata M., McMullen B. A., Miao C. H., Funakoshi T., Hendrickson L. E., Fujikawa K., *Biochemistry*, **27**, 6268—6276 (1988).
6) Ernst J. D., Hoye E., Blackwood R. A., Jaye D., *J. Clin. Invest.*, **85**, 1065—1071 (1990).
7) Gunteski-Hamblin A. M., Song G., Walsh R. A., Frenzke M., Boivin G. P., Dorn G. W., 2nd, Kaetzel M. A., Horseman N. D., Dedman J. R., *Am. J. Physiol.*, **270**, H1091—1100 (1996).
8) Kubista H., Hawkins T. E., Patel D. R., Haigler H. T., Moss S. E., *Curr. Biol.*, **9**, 1403—1406 (1999).
9) Srivastava M., Atwater I., Glasman M., Leighton X., Goping G., Caohuy H., Miller G., Pichel J., Westphal H., Mears D., Rojas E., Pollard H. B., *Proc. Natl. Acad. Sci. U.S.A.*, **96**, 13783—13788 (1999).
10) Herr C., Smyth N., Ullrich S., Yun F., Sasse P., Hescheler J., Fleischmann B., Lasek K., Brixius K., Schwinger R. H., Fassler R., Schroder R., Noegel A. A., *Mol. Cell. Biol.*, **21**, 4119—4128 (2001).
11) Song G., Harding S. E., Duchen M. R., Tunwell R., O'Gara P., Hawkins T. E., Moss S. E., *Faseb. J.*, **16**, 622—624 (2002).
12) Roviezzo F., Getting S. J., Paul-Clark M. J., Yona S., Gavins F. N., Perretti M., Hannon R., Croxtall J. D., Buckingham J. C., Flower R. J., *J. Physiol. Pharmacol.*, **53**, 541—553 (2002).
13) Hannon R., Croxtall J. D., Getting S. J., Roviezzo F., Yona S., Paul-Clark M. J., Gavins F. N., Perretti M., Morris J. F., Buckingham J. C., Flower R. J., *Faseb. J.*, **17**, 253—255 (2003).
14) Croxtall J. D., Gilroy D. W., Solito E., Choudhury Q., Ward B. J., Buckingham J. C., Flower R. J., *Biochem. J.*, **371**, 927—935 (2003).
15) Rand J. H., *N. Engl. J. Med.*, **340**, 1035—1036 (1999).
16) Niimi S., Hyuga M., Harashima M., Seki T., Ariga T., Kawanishi T., Hayakawa T., *Biol. Pharm. Bull.*, **27**, 1864—1868 (2004).
17) Niimi S., Oshizawa T., Yamaguchi T., Harashima M., Seki T., Ariga T., Kawanishi T., Hayakawa T., *Biochem. Biophys. Res. Commun.*, **300**, 770—774 (2003).
18) Kaetzel M. A., Hazarika P., Dedman J. R., *J. Biol. Chem.*, **264**, 14463—14470 (1989).
19) Comera C., Rothhut B., Cavadore J. C., Vilgrain I., Cochet C., Chambaz E., Russo-Marie F., *J. Cell. Biochem.*, **40**, 361—370 (1989).
20) Kristensen B. I., Kristensen P., Johnsen A. H., *Int. J. Biochem.*, **25**, 1195—1202 (1993).
21) Pepinsky R. B., Tizard R., Mattaliano R. J., Sinclair L. K., Miller G. T., Browning J. L., Chow E. P., Burne C., Huang K. S., Pratt D., Wachter L., Hession C., Frey A. Z., Wallner B. P., *J. Biol. Chem.*, **263**, 10799—10811 (1988).
22) Tanaka K., Sato M., Tomita Y., Ichihara A., *J. Biochem.* (Tokyo), **84**, 937—946 (1978).
23) Romisch J., Schuler E., Bastian B., Burger T., Dunkel F. G., Schwinn A., Hartmann A. A., Paques E. P., *Blood Coagul. Fibrinolysis*, **3**, 11—17 (1992).
24) Uno S., Nakamura M., Seki T., Ariga T., *Biochem. Biophys. Res. Commun.*, **239**, 123—128 (1997).
25) Niimi S., Horikawa M., Seki T., Ariga T., Kobayashi T., Hayakawa T., *Biol. Pharm. Bull.*, **25**, 437—440 (2002).
26) Bradford M. M., *Anal. Biochem.*, **72**, 248—254 (1976).
27) Fausto N., Laird A. D., Webber E. M., *Faseb. J.*, **9**, 1527—1536 (1995).
28) Michalopoulos G. K., DeFrances M. C., *Science*, **276**, 60—66 (1997).
29) Liang R. C., Neo J. C., Lo S. L., Tan G. S., Seow T. K., Chung M. C., *J. Chromatogr. B Analyt. Technol. Biomed. Life Sci.*, **771**, 303—328 (2002).
30) de Coupade C., Gillet R., Bennoun M., Briand P., Russo-Marie F.,

Solito E., *Hepatology*, **31**, 371—380 (2000).
31) Masaki T., Tokuda M., Fujimura T., Ohnishi M., Tai Y., Miyamoto K., Itano T., Matsui H., Watanabe S., Sogawa K., Yamada T., Konishi R., Nishioka M., Hatase O., *Hepatology*, **20**, 425—435 (1994).
32) Masaki T., Tokuda M., Ohnishi M., Watanabe S., Fujimura T., Miyamoto K., Itano T., Matsui H., Arima K., Shirai M., Maeba T., Sogawa K., Konishi R., Taniguchi K., Hatanaka Y., Hatase O., Nishioka M., *Hepatology*, **24**, 72—81 (1996).
33) Adachi T., Nakashima S., Saji S., Nakamura T., Nozawa Y., *Hepatology*, **21**, 1668—1674 (1995).
34) Kim S. W., Rhee H. J., Ko J., Kim Y. J., Kim H. G., Yang J. M., Choi E. C., Na D. S., *J. Biol. Chem.*, **276**, 15712—15719 (2001).

Glycobiology vol. 15 no. 5 pp. 447–462, 2005
doi:10.1093/glycob/cwi033
Advance Access publication on December 22, 2004

Site-specific glycosylation analysis of human apolipoprotein B100 using LC/ESI MS/MS

Akira Harazono[1], Nana Kawasaki, Toru Kawanishi, and Takao Hayakawa

National Institute of Health Sciences, Division of Biological Chemistry and Biologicals, 1-18-1 Kami-yoga, Setagaya-Ku, Tokyo 158-8501, Japan

Received on 28 June 2004; revised on 24 November 2004; accepted on 16 December, 2004

Human apolipoprotein B100 (apoB100) has 19 potential *N*-glycosylation sites, and 16 asparagine residues were reported to be occupied by high-mannose type, hybrid type, and monoantennary and biantennary complex type oligosaccharides. In the present study, a site-specific glycosylation analysis of apoB100 was carried out using reversed-phase high-performance liquid chromatography coupled with electrospray ionization tandem mass spectrometry (LC/ESI MS/MS). ApoB100 was reduced, carboxymethylated, and then digested by trypsin or chymotrypsin. The complex mixture of peptides and glycopeptides was subjected to LC/ESI MS/MS, where product ion spectra of the molecular ions were acquired data-dependently. The glycopeptide ions were extracted and confirmed by the presence of carbohydrate-specific fragment ions, such as *m/z* 204 (HexNAc) and 366 (HexHexNAc), in the product ion spectra. The peptide moiety of glycopeptide was determined by the presence of the b- and y-series ions derived from its amino acid sequence in the product ion spectrum, and the oligosaccharide moiety was deduced from the calculated molecular mass of the oligosaccharide. The heterogeneity of carbohydrate structures at 17 glycosylation sites was determined using this methodology. Our data showed that Asn2212, not previously identified as a site of glycosylation, could be glycosylated. It was also revealed that Asn158, 1341, 1350, 3309, and 3331 were occupied by high-mannose type oligosaccharides, and Asn 956, 1496, 2212, 2752, 2955, 3074, 3197, 3438, 3868, 4210, and 4404 were predominantly occupied by mono- or disialylated oligosaccharides. Asn3384, the nearest N-glycosylation site to the LDL-receptor binding site (amino acids 3359–3369), was occupied by a variety of oligosaccharides, including high-mannose, hybrid, and complex types. These results are useful for understanding the structure of LDL particles and oligosaccharide function in LDL–receptor ligand binding.

Key words: apolipoprotein B100/glycopeptide/liquid chromatography electrospray mass spectrometry/product ion spectrum/*N*-linked oligosaccharide

[1]To whom correspondence should be addressed; e-mail: harazono@nihs.go.jp

Introduction

Low-density lipoprotein (LDL) is the main cholesterol carrier in human plasma, and a high serum level of LDL is involved in the development of atherosclerosis. LDL is originally secreted as very low-density lipoprotein (VLDL). VLDL is converted to LDL and then removed from the circulation. Apolipoprotein B100 (apoB100) is the only protein component of LDL and is the ligand recognized by the LDL receptor. The amino acid sequence of human apoB100 has been deduced by analysis of the apoB100 cDNA sequence (Chen *et al.*, 1986; Knott *et al.*, 1986; Law *et al.*, 1986; Yang *et al.*, 1986). Mature apoB100 consists of 4536 amino acids, and its molecular weight has been calculated to be 513 kDa. ApoB100 has 19 potential *N*-glycosylation sites (Asn-X-Ser/Thr), of which 16 asparagine residues are found to be glycosylated (Yang *et al.*, 1989). The carbohydrate moieties were linked to asparagine residues at the following 16 positions: 158, 956, 1341, 1350, 1496, 2752, 2955, 3074, 3197, 3309, 3331, 3384, 3438, 3868, 4210, and 4404. The carbohydrate structures of the *N*-linked sugar chains of human apoB100 were reported to be high-mannose, hybrid, and mono- and disialylated complex type oligosaccharides (Garner *et al.*, 2001; Taniguchi *et al.*, 1979).

The role of carbohydrate moieties of apoB100 has been investigated by several laboratories. The *N*-linked oligosaccharides at the amino terminus of human apoB100 are important for the assembly and secretion of VLDL (Vukmirica *et al.*, 2002). Seven of the *N*-glycans are predicted to occur close to the LDL–receptor binding region of apoB100 and seem to have an important role (Yang *et al.*, 1986, 1989). The carbohydrate composition of apoB100, particularly sialylation, has been considered to contribute to the atherogenic properties of LDL. However, Shireman and Fisher (1979) reported that they do not appear to play a significant role in the binding of apoB100 to the LDL receptor. Furthermore, the distribution and diversity of human apoB100 oligosaccharides isolated from normolipidemic, hypercholesterolemic, and hypertriglyceridemic diabetic subjects were highly conserved even when characterized in LDL subfractions (Garner *et al.*, 2001). The potential function of apoB100 carbohydrates posthepatic secretion is not well understood. Glycoproteins have a variety of sugar chains at each glycosylation site. Because of the individual functions at each site, a comparison of glycosylation among various sites is important. Therefore, to investigate the role of carbohydrate moieties of apoB100, we attempted to determine the carbohydrate heterogeneity site-specifically.

To determine the site-specific carbohydrate heterogeneity of glycoproteins, the glycoprotein must be digested into

peptides and glycopeptides, and then both the peptide and sugar chain of each glycopeptide must be analyzed. One of the most effective techniques for mapping proteolytic fragments of glycoproteins is liquid chromatography (LC) coupled with electrospray ionization (ESI) mass spectrometry (MS) (Carr *et al.*, 1993; Duffin *et al.*, 1992; Kawasaki *et al.*, 2004; Ling *et al.*, 1991). The specific detection of glycopeptides can be achieved by monitoring specific diagnostic sugar oxonium ions, such as *m/z* 204 (HexNAc) and 366 (HexHexNAc) produced by cone voltage fragmentation, or by precursor ion scanning (Carr *et al.*, 1993; Duffin *et al.*, 1992). However, when many *N*-glycosylation sites are present within a glycoprotein, the chromatogram becomes extremely complex and assignment of the glycopeptide ions is very difficult.

We present here an alternative strategy for the site-specific glycosylation analysis of a peptide and glycopeptide mixture using LC/ESI MS/MS, where we acquired the product ion spectrum for all significant molecular ions in a data-dependent manner. Product ion spectra of molecular ions allow the specific detection of glycopeptides from a complex mixture of peptides based on the presence of diagnostic sugar oxonium ions of oligosaccharides. Furthermore, this method allows confirmation of the amino acid sequence of a glycopeptide by the presence of b- and y-series fragment ions of the peptide. Using this method, we identified one previously unidentified *N*-glycosylated site of ApoB100 and determined the oligosaccharide heterogeneity of each of 17 *N*-glycosylation sites. Our findings provide information on the structure of apoB100 that will be useful to future studies on the structure, function, and metabolism of plasma LDL.

Results

Enzyme digestion

To determine the oligosaccharide heterogeneity at each glycosylation site, reduced and carboxymethylated apoB100 was digested into peptides and glycopeptides. Table I shows the amino acid sequences of the tryptic or chymotryptic peptides, including the putative *N*-glycosylation sites. The putative glycosylation sites were numbered (G1–19). Boldface indicates the previously reported *N*-glycosylation sites (G2–6 and G9–19). When apoB100 is digested by trypsin, potential *N*-glycosylation sites, Asn1341 (G4) and Asn1350 (G5), belong to the same peptide. Because chymotrypsin

Table I. The amino acid sequences of the tryptic or chymotryptic peptides including the putative *N*-glycosylation sites in apoB100

N-glycosylation site[a]		Tryptic digests		Chymotryptic digests	
Residue	ID	Sequence	Theoretical mass[b]	Sequence	Theoretical mass[b]
Asn[7]	G1	EEEMLEN[7]VSLVCPK	1677.8	EN[7]VSL	560.3
Asn[158]	**G2**	QVLFLDTVYGN[158]CSTHFTVK	2229.1	GN[158]CSTHF	822.3
Asn[956]	**G3**	QVFPGLNYCTSGAYSN[956]ASSTDSASYYPLTGDTR	3550.5	SN[956]ASSTDSASY	1088.4
Asn[1341]	**G4**	LYQLQVPLLGVLDLSTNVYSNLYN[1341]	4692.3	N[1341]W	318.1
Asn[1350]	**G5**	WSASYSGGN[1350]TSTDHFSLR		SGGN[1350]TSTDHF	1021.4
Asn[1496]	**G6**	FN[1496]SSYLQGTNQITGR	1684.8	N[1496]SSY	469.2
Asn[2212]	G7	TIHDLHLFIENIDFN[2212]K	1968.0	N[2212]KSGSSTASW	1023.5
Asn[2533]	G8	N[2533]LTDFAEQYSIQDWAK	1928.9	AAKN[2533]L	515.3
Asn[2752]	**G9**	IQSPLFTLDANADIGN[2752]GTTSANEAGIAASITAK	3231.6	DANADIGN[2752] GTTSANEAGIAASITAKGESKL	2846.4
Asn[2955]	**G10**	VNQNLVYESGSLN[2955]FSK	1797.9	N[2955]F	279.1
Asn[3074]	**G11**	YNQN[3074]FSAGNNENIMEAHVGINGEANLD FLNIPLTIPEMR	4359.1	NQN[3074]F	521.2
Asn[3197]	**G12**	SYN[3197]ETK	740.3	N[3197]ETKIKF	878.5
Asn[3309]	**G13**	ELCTISHIFIPAMGN[3309]ITYDFSFK	2704.3	IPAMGN[3309]ITY	978.5
Asn[3331]	**G14**	SSVITLNTNAELFN[3331]QSDIVAHLLSSSSSVIDALQYK	3864.0	N[3331]QSDIVAHL	995.5
Asn[3384]	**G15**	FVEGSHN[3384]STVSLTTK	1605.8	VEGSHN[3384]STVSL	1128.5
Asn[3438]	**G16**	YDFN[3438]SSMLYSTAK	1525.7	N[3438]SSML	550.2
Asn[3868]	**G17**	FEVDSPVYN[3868]ATWSASLK	1912.9	N[3868]ATW	490.2
Asn[4210]	**G18**	VHN[4210]GSEILFSYFQDLVITLPFELR	2836.5	SKVHN[4210]GSEIL	1082.6
Asn[4404]	**G19**	DFHSEYIVSASN[4404]FTSQLSSQVEQFLHR	3155.5	IVSASN[4404]F	736.4

Human apoB100 amino acid sequence (NP_000375. apolipoprotein B [gi:4502153]) was obtained from the NCBI database (www.ncbi.nlm.nih.gov/pubmed). Boldface indicates previously reported *N*-glycosylation sites. Cystein residue was carboxymethylated, and carboxymethylated cystein was underscored.

[a]Potential *N*-glycosylation sites were identified with the consensus sequence NXS/T, where X is any amino acid except P.

[b]Monoisotopic mass value.

can cleave apoB100 into glycopeptides containing one glycosylation site, we attempted to analyze both proteolytic fragments from trypsin digestion and chymotrypsin digestion to identify the site-specific glycosylation.

LC/ESI MS/MS analysis of tryptic digest of apoB100

The schema of a site-specific glycosylation analysis of apoB100 is shown in Figure 1. A mixture of peptides and glycopeptides was subjected to LC/ESI MS/MS with a reversed-phase column. Figure 2A shows a total ion chromatogram (TIC) of a time-of-flight (TOF) MS scan for the full scan *m/z* 1000–2000. When double or higher charged molecular ions were detected, the product ion spectrum was automatically acquired. Figure 2B shows a TIC of the product ion scan. The collision energy at the second quadrupole for the product ion scan was adjusted from 50 to 80 eV depending on the size and charge of the precursor ion. Under these conditions, peptide precursor ions produced b- and y-series fragment ions derived from its amino acid sequence (data not shown), and glycopeptide precursor ions produced abundant carbohydrate-specific ions, *m/z* 204, 186, 168, and 366 (described later). The intensity of ions at *m/z* 204.05–204.15 (HexNAc, 204.08) in each product ion scan are illustrated in Figure 2C. The extracted ion chromatogram at *m/z* 204 (Figure 2C) and 366 (data not shown) provides useful information on the selection of glycopeptide precursor ions. The product ion spectra of glycopeptides show a very characteristic pattern (see later figures). There were intense oligosaccharide-derived peaks of *m/z* 204 (HexNAc), 366 (HexHexNAc), 186 (HexNAc–H_2O), and 168 (HexNAc–$2H_2O$), and if present, 163 (Hex), 292 (Neu5Ac), and 274 (Neu5Ac–H_2O). Therefore, we can very easily distinguish the glycopeptide precursor ions from peptide ions. As expected, many parent ions having 204 and

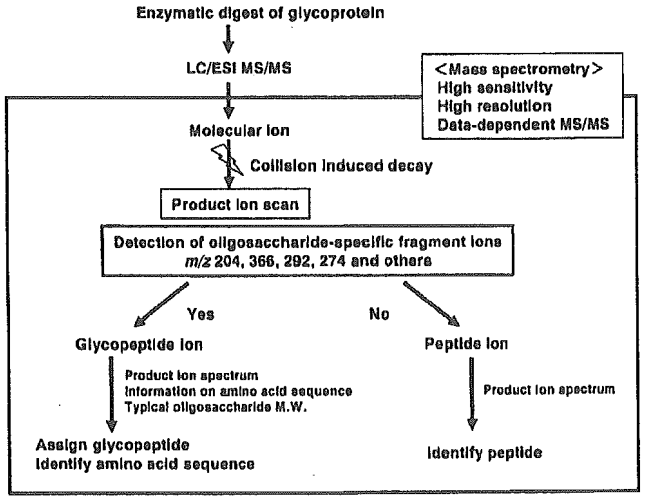

Fig. 1. Schema of site-specific glycosylation analysis. Glycoprotein was digested into peptides and glycopeptides containing only one glycosylation site. Only LC/ESI MS/MS was used. Data-dependent MS/MS acquisition was used to differentiate glycopeptide ions from peptide ions and identify the amino acid sequence of the glycopeptides. The oligosaccharide structure was deduced based on the calculated oligosaccharide molecular weight.

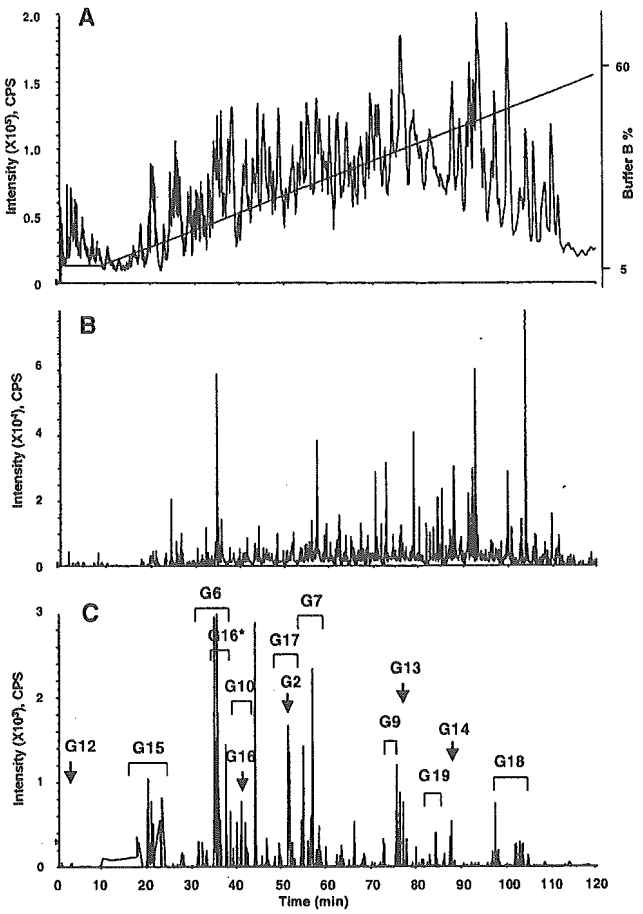

Fig. 2. LC/ESI MS/MS of tryptic digest of apolipoprotein B100. TIC of the TOF MS scan for the full scan *m/z* 1000–2000 and the HPLC gradient are indicated (**A**). TIC of the product ion scan data-dependently acquired (**B**). Extract ion chromatogram at *m/z* 204 of product ion spectra (**C**). Arrows and brackets denote glycopeptide fraction and *N*-glycosylation site ID. G16* was found to be oxidized at a methionine residue.

366 fragment ions in the product ion spectrum were detected, and most of these precursor ions were found as glycopeptides.

The glycopeptides were assigned based on an examination of product ion spectra using the information on the peptides containing a putative *N*-glycosylation site. Figures 3A, 3B, and 3C show the product ion spectra of 1412.1 (+2) at 18 min, 1160.4 (+3) at 20 min and 1271.1 (+3) at 22 min for the glycopeptides. There were intense carbohydrate B^+ ions such as *m/z* 204 (HexNAc), 366 (HexHexNAc), and 186 (HexNAc–H_2O) and other weak peaks in the product ion spectra. These product ion spectra were very similar to each other (Figure 3A, 3B, and 3C). Careful examination of these product ion spectra for the glycopeptides revealed that several fragment ions were consistent with b- and y-series fragment ions derived from the peptide FVEGSHNSTVSLTTK (residue 3378–3392). The deduced b- and y-series fragment ions of the peptide FVEGSHNSTVSLTTK were listed, and the fragment ions detected in the product ion spectrum of 1160.4 (+3) are underscored in the table (Figure 3D). The molecular ions of the peptide (*m/z* 1606) and

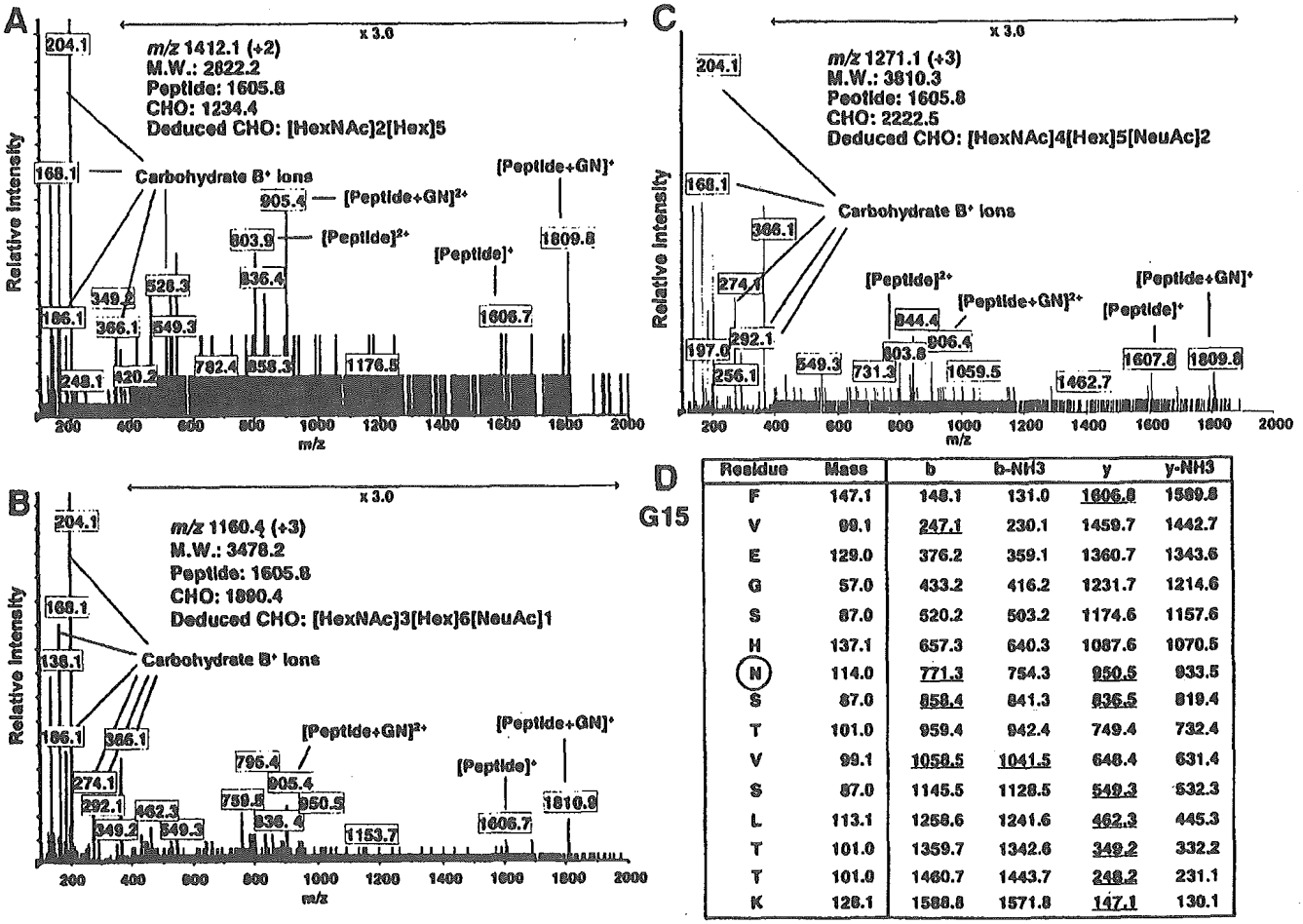

D

G15

Residue	Mass	b	b-NH3	y	y-NH3
F	147.1	148.1	131.0	1606.8	1589.8
V	99.1	247.1	230.1	1459.7	1442.7
E	129.0	376.2	359.1	1360.7	1343.6
G	57.0	433.2	416.2	1231.7	1214.6
S	87.0	520.2	503.2	1174.6	1157.6
H	137.1	657.3	640.3	1087.6	1070.5
(N)	114.0	771.3	754.3	950.5	933.5
S	87.0	858.4	841.3	836.5	819.4
T	101.0	959.4	942.4	749.4	732.4
V	99.1	1058.5	1041.5	648.4	631.4
S	87.0	1145.5	1128.5	549.3	532.3
L	113.1	1258.6	1241.6	462.3	445.3
T	101.0	1359.7	1342.6	349.2	332.2
T	101.0	1460.7	1443.7	248.2	231.1
K	128.1	1588.8	1571.8	147.1	130.1

Fig. 3. Product ion spectra of the *N*-glycosylated peptides containing Asn3384 (G15). Product ion scan of *m/z* 1412.1 (+2) (**A**), 1160.4 (+3) (**B**), and 1271.1 (+3) (**C**) at 18, 20, and 22 min, respectively. These spectra show a characteristic fragmentation pattern with abundant carbohydrate-diagnostic oxonium ions at 163, 168, 186, 204, and 366 and very similar patterns to each other. The oxonium ions at m/z 292 (Neu5Ac) and 274 (Neu5A-H2O) were observed in the peptides having sialylated oligosaccharide (**B**) and (**C**). Several fragment ions are consistent with the b- and y-series fragment ions derived from the peptide FVEGSHNSTVSLTTK (residue 3378–3392). $[Peptide]^+$ and $[peptide+GlcNAc]^+$ ions were also detected. (**D**) shows *m/z* of the proposed b- and y-series fragment ions of the peptide and the fragment ions detected in Figure 3B are underscored. Based on the calculated oligosaccharide mass, the deduced oligosaccharide structure was presented. GN, *N*-acetylglucosamine.

peptide + GlcNAc (*m/z* 1809) were also detected in the product ion spectra (Figure 3A, 3B, and 3C). These results suggest that these glycopeptides have the same peptide, FVEGSHNSTVSLTTK, including the *N*-glycosylation site Asn3384 (G15). Carbohydrate molecular weight was calculated by subtracting the theoretical molecular weight of the peptide (1605.8) from the calculated molecular weight of the glycopeptide and adding the molecular weight of H_2O (18.0). The oligosaccharide structure was deduced based on the molecular weight and previously reported oligosaccharides of apoB100. The presence of product ions at *m/z* 274 (Neu5Ac–H_2O) and 292 (Neu5Ac) suggested that those at *m/z* 1160.4 (+3) and 1271.1 (+3) were glycopeptide ions having sialylated oligosaccharides. Thus the carbohydrate compositions, $[HexNAc]_2[Hex]_5$, $[HexNAc]_3[Hex]_6[Neu5Ac]_1$, and $[HexNAc]_4[Hex]_5[Neu5Ac]_2$, were deduced from the carbohydrate molecular weights, 1234.4, 1890.4, and 2222.5, respectively.

Figures 4 shows the product ion spectra of 1294.8 (+3) at 55 min and 1152.7 (+3) at 35 min for other glycopeptides. There are intense carbohydrate B^+ ions in the product ion spectra. Several ions consisting of b- and y-series fragment ions from the peptide TIHDLHLFIENIDHNK (residue 2198–2213) were found in the product ion spectrum of 1294.8 (+3) (Figure 4A), and detected ions are underscored in the table. The molecular ions of the peptide (*m/z* 1968.9) were also detected in the product ion spectra. The carbohydrate molecular weight was calculated from the molecular weight of the peptide, 1968.0, and the molecular weight of the glycopeptide, 3881.4. Carbohydrate composition was deduced from the carbohydrate molecular weight (1931.4) and presence of Neu5Ac. Thus, the peptide moiety TIHDLHLFIENIDHNK and carbohydrate composition $[HexNAc]_4[Hex]_5[Neu5Ac]_1$ were suggested.

Many ions in the product ion spectrum of 1152.7 (+3) were consistent with the b- and y-series fragment ions

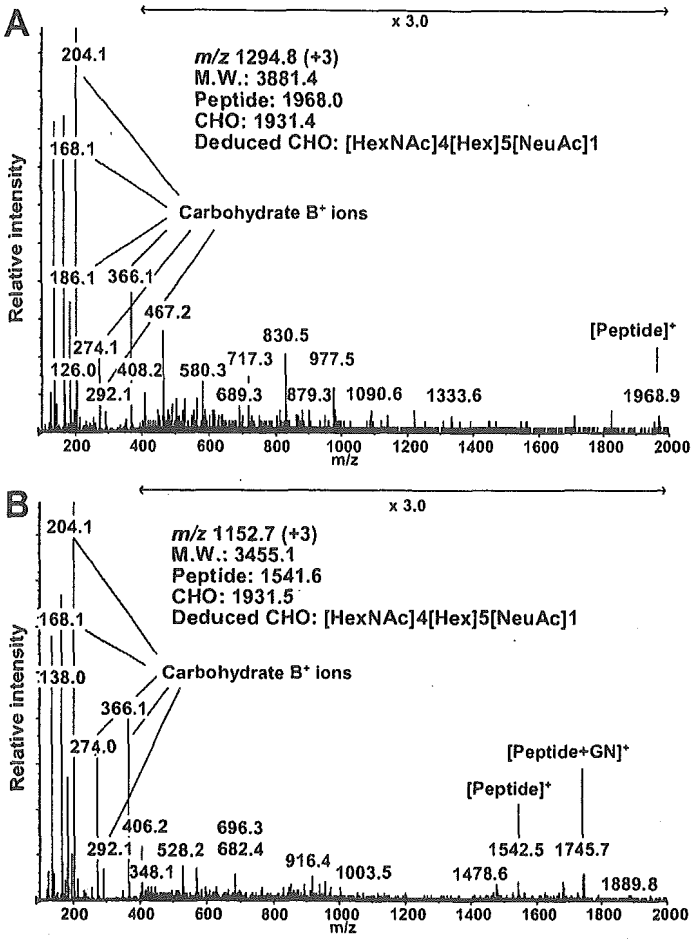

G7

Residue	Mass	b	b-NH3	y	y-NH3
T	101.0	102.1	85.0	1969.0	1952.0
I	113.1	215.1	198.1	1868.0	1850.9
H	137.1	352.2	335.2	1754.9	1737.9
D	115.0	467.2	450.2	1617.8	1600.8
L	113.1	580.3	563.3	1502.8	1485.8
H	137.1	717.4	700.3	1389.7	1372.7
L	113.1	830.5	813.4	1252.7	1235.6
F	147.1	977.5	960.5	1139.6	1122.5
I	113.1	1090.6	1073.6	992.5	975.5
E	129.0	1219.6	1202.6	879.4	862.4
N	114.0	1333.7	1316.7	750.4	733.4
I	113.1	1446.8	1429.7	636.3	619.3
D	115.0	1561.8	1544.8	523.3	506.2
F	147.1	1708.9	1691.8	408.2	391.2
(N)	114.0	1822.9	1805.9	261.2	244.1
K	128.1	1951.0	1934.0	147.1	130.1

G16

Residue	Mass	b	b-NH3	y	y-NH3
Y	163.1	164.1	147.0	1542.7	1525.7
D	115.0	279.1	262.1	1379.6	1362.6
F	147.1	426.2	409.1	1264.6	1247.6
(N)	114.0	540.2	523.2	1117.5	1100.5
S	87.0	627.2	610.2	1003.5	986.5
S	87.0	714.3	697.2	916.4	899.4
M(O)	147.0	861.3	844.3	845.4	828.4
L	113.1	974.4	957.4	682.4	665.4
Y	163.1	1137.5	1120.4	569.3	552.3
S	87.0	1224.5	1207.5	406.2	389.2
T	101.0	1325.5	1308.5	319.2	302.2
A	71.0	1396.6	1379.6	218.1	201.1
K	128.1	1524.7	1507.6	147.1	130.1

Fig. 4. Product ion spectra of the tryptic *N*-glycosylated peptides of apoB100. (**A**) Product ion spectrum of *m/z* 1294.8 (+3) at 55 min for the glycopeptide containing Asn2212 (G7). Several ions are consistent with the b- and y-series fragment ions derived from the peptide TIHDLHLFIENIDFNK (residue 2198–2213). Table shows *m/z* of the proposed b- and y-series fragment ions and the detected ions are underscored. (**B**) Product ion spectrum of *m/z* 1152.7 (+3) at 35 min for the glycopeptide containing Asn3438 (G16) with oxidized methionine. The methionine residue at 3441 was considered oxidized. Several ions are consistent with the b- and y-series fragment ions derived from the peptide YDFNSSM(O)LYSTAK (residue 3435–3447). Table shows *m/z* of the proposed b- and y-series fragment ions and the detected ions are underscored. M(O), oxidized methionine.

derived from the peptide YSFNSSMLYSTAK (Figure 4B). However, the deduced peptide ion *m/z* at 1526.7 and peptide + GlcNAc at 1729.8 were not detected. The difference of 203 between the product ions at *m/z* 1542.5 and 1745.7 suggests that the molecular weight of the peptide moiety may be 1541.5, and an increase in mass of 16 Da suggests that the methionine residue of YSFNSSMLYSTAK (residue 3435–3447, molecular weight 1525.7) was oxidized. The deduced b- and y-series fragment ions of the peptide, YSFNSSMLYSTAK, with the oxidized methionine are listed and detected peptide fragment ions are underscored. Thus, the product ions at *m/z* 1542.5 and 1745.7 were considered the peptide and peptide + GlcNAc ions, respectively. Our method identified unexpected oxidization of methionine residue (Figure 4B). The carbohydrate molecular weight was calculated, and the carbohydrate composition, $[HexNAc]_4[Hex]_5[Neu5Ac]_1$, was deduced from the carbohydrate molecular weight, 1931.4, and presence of Neu5Ac.

Results of site-specific glycosylation analysis from tryptic digest are summarized in Table II. To avoid misassignment, only ions that were confirmed as glycopeptides by the product ion spectra or coeluting ions with glycopeptides were listed. We determined 13 of the 19 potential *N*-glycosylation sites and the oligosaccharide heterogeneity at each site in a site-specific glycosylation analysis of the tryptic digest of apoB100. The type of oligosaccharide was deduced based on the oligosaccharide composition. Glycopeptides containing *N*-glycosylation sites Asn7, 956, 1341, 1350, 2533, and 3074 (G1, 3, 4, 5, 8, and 11) could not be detected. The relative peak intensity does not accurately express the relative amount of glycoforms, because of the different ionization efficiency of each glycoform, different detection sensitivity at *m/z*, and simultaneous acquision of MS and MS/MS spectra. However, the relative peak intensity of each glycopeptide would provide an indication of the distribution in glycoforms.

Table II. Site-specific glycosylation analysis of the tryptic digest of apoB100 using LC/ESI MS/MS

			Glycopeptides			Oligosaccharide				
Glycosylation site ID	Retention time (min)	Peptide theoretical MW[a]	*m/z*	Charge	Calculated MW[a]	Calculated MW[a]	Theoretical MW[a]	Relative peak intensity (%)[b]	Composition[c]	Deduced Type[c]
G1	—	1677.8	—	—	—	—	—	—	—	—
G2	51	2229.1	1365.6	+3	4093.8	1882.7	1882.6	7	[HexNAc]2[Hex]9	High mannose
	51	2229.1	1311.6	+3	3931.7	1720.6	1720.6	13	[HexNAc]2[Hex]8	High mannose
	51	2229.1	1257.5	+3	3769.5	1558.4	1558.5	22	[HexNAc]2[Hex]7	High mannose
	51	2229.1	1203.5	+3	3607.6	1396.6	1396.5	13	[HexNAc]2[Hex]6	High mannose
	51	2229.1	1149.5	+3	3445.5	1234.4	1234.4	100	[HexNAc]2[Hex]5	High mannose
	51	2229.1	1723.7	+2	3445.4	1234.4				
G3	—	3550.5	—	—	—	—	—	—	—	—
G4, G5	—	4692.3	—	—	—	—	—	—	—	—
G6	33	1684.8	1451.6	+2	2901.2	1234.4	1234.4	15	[HexNAc]2[Hex]5	High mannose
	34	1684.8	1200.4	+3	3598.2	1931.4	1931.7	100	[HexNAc]4[Hex]5[Neu5Ac]1	Biantennary complex
	34	1684.8	1800.1	+2	3598.2	1931.4				
	35	1684.8	1146.4	+3	3436.2	1769.4	1769.6	23	[HexNAc]4[Hex]4[Neu5Ac]1	Biantennary complex
	35	1684.8	1719.2	+2	3436.4	1769.6				
	35	1684.8	1078.7	+3	3233.1	1566.3	1566.6	11	[HexNAc]3[Hex]4[Neu5Ac]1	Monoantennary complex
	35	1684.8	1132.8	+3	3395.4	1728.6	1728.6	5	[HexNAc]3[Hex]5[Neu5Ac]1	Hybrid
	35	1684.8	1186.8	+3	3557.4	1890.6	1890.7	3	[HexNAc]3[Hex]6[Neu5Ac]1	Hybrid
	35	1684.8	1240.8	+3	3719.4	2052.6	2052.7	3	[HexNAc]3[Hex]7[Neu5Ac]1	Hybrid
	37	1684.8	1297.4	+3	3889.2	2222.4	2222.8	24	[HexNAc]4[Hex]5[Neu5Ac]2	Biantennary complex
	37	1684.8	1945.7	+2	3889.4	2222.6				
G7	54	1968.0	1294.8	+3	3881.4	1931.4	1931.7	66	[HexNAc]4[Hex]5[Neu5Ac]1	Biantennary complex
	58	1968.0	1044.2	+4	4172.8	2222.8	2222.8	100	[HexNAc]4[Hex]5[Neu5Ac]2	Biantennary complex
	58	1968.0	1391.9	+3	4172.7	2222.7				
G8	—	1928.9	—	—	—	—	—	—	—	—
G9	73	3231.6	1360.4	+4	5437.6	2224.0	2222.8	—	[HexNAc]4[Hex]5[Neu5Ac]2	Biantennary complex
G10	40	1797.9	1238.1	+3	3711.3	1931.4	1931.7	41	[HexNAc]4[Hex]5[Neu5Ac]1	Biantennary complex
	41	1797.9	1856.7	+2	3711.4	1931.5				

Table II. continued

Glycosylation site ID	Retention time (min)	Peptide theoretical MW[a]	Glycopeptides *m/z*	Charge	Calculated MW[a]	Oligosaccharide Calculated MW[a]	Theoretical MW[a]	Relative peak intensity (%)[b]	Composition[c]	Deduced Type[c]
	43	1797.9	1001.6	+4	4002.4	2222.5	2222.8	100	[HexNAc]4[Hex]5[Neu5Ac]2	Biantennary complex
	43	1797.9	1335.1	+3	4002.3	2222.4				
G11	—	4359.1	—	—	—	—	—	—	—	—
G12	2	740.3	1473.6	+2	2945.2	2222.9	2222.8	—	[HexNAc]4[Hex]5[Neu5Ac]2	Biantennary complex
G13	75	2704.3	1102.7	+4	4406.8	1720.5	1720.6	22	[HexNAc]2[Hex]8	High mannose
	75	2704.3	1470.0	+3	4406.9	1720.6				
	76	2704.3	1062.2	+4	4244.8	1558.5	1558.5	54	[HexNAc]2[Hex]7	High mannose
	76	2704.3	1415.9	+3	4244.7	1558.4				
	76	2704.3	1021.6	+4	4082.4	1396.1	1396.5	100	[HexNAc]2[Hex]6	High mannose
	76	2704.3	1361.9	+3	4082.7	1396.4				
	76	2704.3	1307.9	+3	3920.7	1234.4	1234.4	50	[HexNAc]2[Hex]5	High mannose
G14	88	3864.0	1146.7	+5	5728.7	1882.7	1882.6	—	[HexNAc]2[Hex]9	High mannose
	88	3864.0	1433.1	+4	5728.3	1882.3				
G15	17	1605.8	1063.4	+3	3187.2	1599.4	1599.6	8	[HexNAc]3[Hex]6	Hybrid
	17	1605.8	1077.0	+3	3228.0	1640.2	1640.6	20	[HexNAc]4[Hex]5	Biantennary complex
	17	1605.8	1009.4	+3	3025.2	1437.4	1437.5	20	[HexNAc]3[Hex]5	Hybrid
	18	1605.8	1513.6	+2	3025.3	1437.5				
	18	1605.8	1023.0	+3	3066.0	1478.2	1478.5	13	[HexNAc]4[Hex]4	Biantennary complex
	18	1605.8	1412.1	+2	2822.2	1234.4	1234.4	4	[HexNAc]2[Hex]5	High mannose
	20	1605.8	1174.1	+3	3519.3	1931.5	1931.7	100	[HexNAc]4[Hex]5[Neu5Ac]1	Biantennary complex
	20	1605.8	1760.7	+2	3519.4	1931.6				
	20	1605.8	1160.4	+3	3478.2	1890.4	1890.7	10	[HexNAc]3[Hex]6[Neu5Ac]1	Hybrid
	20	1605.8	1106.4	+3	3316.2	1728.4	1728.6	94	[HexNAc]3[Hex]5[Neu5Ac]1	Hybrid
	20	1605.8	1659.2	+2	3316.4	1728.6				
	20	1605.8	1222.8	+3	3665.4	2077.6	2077.7	4	[HexNAc]4[Hex]5[Neu5Ac]1[Fuc]1	Biantennary complex
	20	1605.8	1052.4	+3	3154.2	1566.4	1566.6	42	[HexNAc]3[Hex]4[Neu5Ac]1	Monoantennary complex
	20	1605.8	1578.2	+2	3154.4	1566.6				
	21	1605.8	1120.0	+3	3357.0	1769.2	1769.6	23	[HexNAc]4[Hex]4[Neu5Ac]1	Biantennary complex
	22	1605.8	1271.1	+3	3810.3	2222.5	2222.8	49	[HexNAc]4[Hex]5[Neu5Ac]2	Biantennary complex
G16	42	1525.7	1147.4	+3	3439.2	1931.5	1931.7	—	[HexNAc]4[Hex]5[Neu5Ac]1	Biantennary complex
	42	1525.7	1720.7	+2	3439.3	1931.6				
	35	1541.7*	1152.7	+3	3455.1	1931.4	1931.7	100	[HexNAc]4[Hex]5[Neu5Ac]1	Biantennary complex

Table II. continued

Glycosylation site ID	Retention time (min)	Peptide theoretical MW[a]	Glycopeptides			Oligosaccharide			Composition[c]	Deduced Type[c]
			m/z	Charge	Calculated MW[a]	Calculated MW[a]	Theoretical MW[a]	Relative peak intensity (%)[b]		
	35	1541.7*	1728.6	+2	3455.2	1931.5				
	36	1541.7*	1098.7	+3	3293.1	1769.4	1769.6	9	[HexNAc]4[Hex]4[Neu5Ac]1	Biantennary complex
	36	1541.7*	1647.6	+2	3293.2	1769.5				
	36	1541.7*	1546.1	+2	3090.2	1566.5	1566.6	18	[HexNAc]3[Hex]4[Neu5Ac]1	Monoantennary complex
	38	1541.7*	1249.8	+3	3746.4	2222.7	2222.8	19	[HexNAc]4[Hex]5[Neu5Ac]2	Biantennary complex
G17	51	1912.9	1276.5	+3	3826.5	1931.6	1931.7	100	[HexNAc]4[Hex]5[Neu5Ac]1	Biantennary complex
	51	1912.9	1914.3	+2	3826.6	1931.7				
	54	1912.9	1495.3	+3	4482.9	2588.0	2587.9	6	[HexNAc]5[Hex]6[Neu5Ac]2	Triantennary complex
	54	1912.9	1030.4	+4	4117.6	2222.7	2222.8	39	[HexNAc]4[Hex]5[Neu5Ac]2	Biantennary complex
	54	1912.9	1373.5	+3	4117.5	2222.6				
G18	98	2836.5	1188.5	+4	4750.2	1931.7	1931.7	100	[HexNAc]4[Hex]5[Neu5Ac]1	Biantennary complex
	98	2836.5	1584.4	+3	4750.1	1931.7				
	98	2836.5	1148.0	+4	4588.1	1769.6	1769.6	10	[HexNAc]4[Hex]4[Neu5Ac]1	Biantennary complex
	102	2836.5	1009.3	+5	5041.3	2222.8	2222.8	64	[HexNAc]4[Hex]5[Neu5Ac]2	Biantennary complex
	102	2836.5	1261.6	+4	5042.2	2223.7				
	103	2836.5	1681.5	+3	5041.5	2223.0				
G19	83	3155.5	1014.8	+5	5069.0	1931.5	1931.7	79	[HexNAc]4[Hex]5[Neu5Ac]1	Biantennary complex
	86	3155.5	1073.1	+5	5360.5	2223.0	2222.8	100	[HexNAc]4[Hex]5[Neu5Ac]2	Biantennary complex

[a]Monoisotopic mass value.
[b]Relative peak intensity was calculated by comparing same charge state glycopeptide ions. The intensity of glycoform with maximum intensity at each glycosylation site was considered as 100%.
[c]The oligosaccharide composition and type were deduced from its composition.
*The glycopeptides including G16 were found to be oxidized at methionine residue.

When each product ion spectrum of the peptide ions in this LC/ESI MS/MS analysis was identified by the computer program Mascot, the sequence coverage of apoB100 was 38%. The ions, *m/z* 1177.9 (+3) at 64 min, 1289.0 (+3) at 91 min, and 1053.2 (+3) at 84 min, were identified as TIHDLHLFIENIDFN^{2212}KSGSSTASWIQNVDTK containing the potential *N*-glycosylation site Asn2212 (G7), SSVITLNTNAELFN^{3331}QSDIVAHLLSSSSSVIDALQYK containing Asn3331 (G14), and DFHSEYIVSASN^{4404}-FTSQLSSQVEQFLHR containing Asn4404 (G19), respectively (data not shown). These results indicate that some parts of these glycosylation sites were not glycosylated. There were many unexplained peptides and glycopeptides in the digest (data not shown). This may be due to the unexpected digestion or nonspecific cleavage of apolipoprotein B100 as well as the multiple isoforms of the proteins.

LC/ESI MS/MS analysis of chymotryptic digest of apoB100

To determine the carbohydrate at undetected glycosylation sites in the tryptic digest including Asn1341 and 1350 (G4 and G5), which belong to the same tryptic peptide, the chymotrypsin digest was analyzed by LC/ESI MS/MS using the same methodology. Figure 5A shows a TIC of the TOF MS scan for the full scan *m/z* 700–2000. The collision energy was adjusted at 40–80 eV depending on the precursor ions. A TIC of the product ion scan and extracted ion chromatogram at *m/z* 204.05–204.15 (HexNAc) are presented in Figure 5B and 5C, respectively.

Figure 6A shows the product ion spectrum of 768.4 (+2) at 14 min for the chymotryptic glycopeptide. The carbohydrate B^+ ions, y1 and b2 ions of peptide NW (residue 1341–1342), and peptide + GlcNAc ion were found in the product ion spectrum. The carbohydrate composition, $[HexNAc]_2[Hex]_5$, was deduced from the calculated carbohydrate molecular ion, 1234.6. Figure 6B shows the product ion spectrum of 1444.1 (+2) at 9 min for the glycopeptide. The carbohydrate B^+ ions, peptide and peptide + GlcNAc ions, and peptide fragment ions from the peptide SGGNTSTDHF (residue 1347–1356) were detected in the product ion spectrum. Carbohydrate molecular weight, 1882.8, was calculated and the oligosaccharide composition, $[HexNAc]_2[Hex]_6$, was deduced from the molecular weight. The peptide fragment ions were also detected in the product ion spectrum for the chymotryptic glycopeptides as tryptic glycopeptides. The peptide and peptide + GlcNAc ions were detected in product ion spectra. These ions helped us determine the peptide moiety of the glycopeptide ion.

Results of the site-specific analysis of glycosylation of the chymotryptic digest are summarized in Table III. The oligosaccharide heterogeneity at each of 13 *N*-glycosylation sites was determined by LC/ESI MS/MS from the chymotryptic digest of apoB100 (Table III).

Carbohydrate diversity of each site

Results for the tryptic digest and chymotryptic digest of apoB100 are listed in Table IV. The oligosaccharide composition and type were deduced based on the molecular weight and previously reported oligosaccharide structures of apoB100. No information on glycosylation at Asn7 and 2533 (G1 and 8) was obtained from the analysis of the

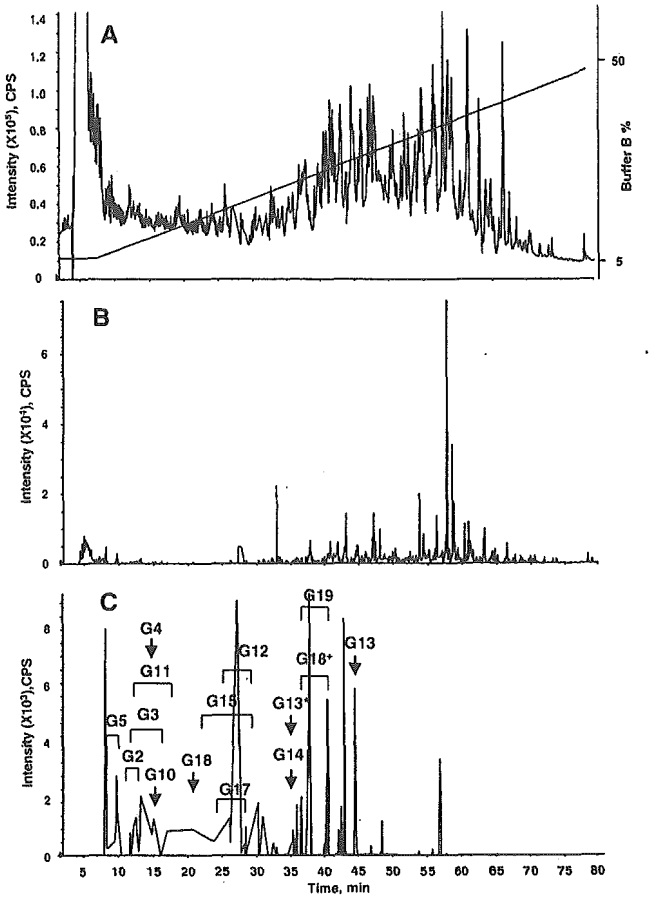

Fig. 5. LC/ESI MS/MS of chymotryptic digest of apolipoprotein B100. TIC of TOF MS scan for the full scan *m/z* 700–2000 and the HPLC gradient are indicated (**A**). TIC of the product ion scan data-dependently acquired (**B**). Extract ion chromatogram at *m/z* 204 of product ion spectra (**C**). Arrows and brackets denote glycopeptide fraction and *N*-glycosylation site ID. G13* was found to be oxidized at a methionine residue. $G18^+$ was found as missed cleaved glycopeptides.

tryptic or chymotryptic digest. When the tryptic digest of apoB100 was analyzed by LC/ESI MS/MS with the MS range *m/z* 400–2000, the sequence coverage of apoB100 was 41% and tryptic peptides containing Asn7, 2212, 2533, or 2955 (G1, 7, 8, or 10) were detected (data not shown). Together with the result of LC/ESI MS/MS with the MS range *m/z* 1000–2000, Asn7 and 2533 (G1 and 8) were not glycosylated or glycosylated only under detection sensitivity, and Asn2212, 2955, 3331, and 4404 (G7, 10, 14, and 19) were partially glycosylated. These findings indicate that 17 of 19 potential *N*-glycosylation sites in apoB100 were glycosylated.

The most heterogeneous oligosaccharides were found at Asn3384 (G15). Asn3384 possessed neutral or monosialylated hybrid and monoantennary complex type and mono- or disialylated biantennary complex type oligosaccharides as well as one high-mannose type oligosaccharide. Asn158, 1341, 1350, 3309, and 3331 (G2, 4, 5, 13, and 14) were occupied by high-mannose type oligosaccharides, whereas Asn956, 1496, 2212, 2752, 2955, 3074, 3197, 3438, 3868,

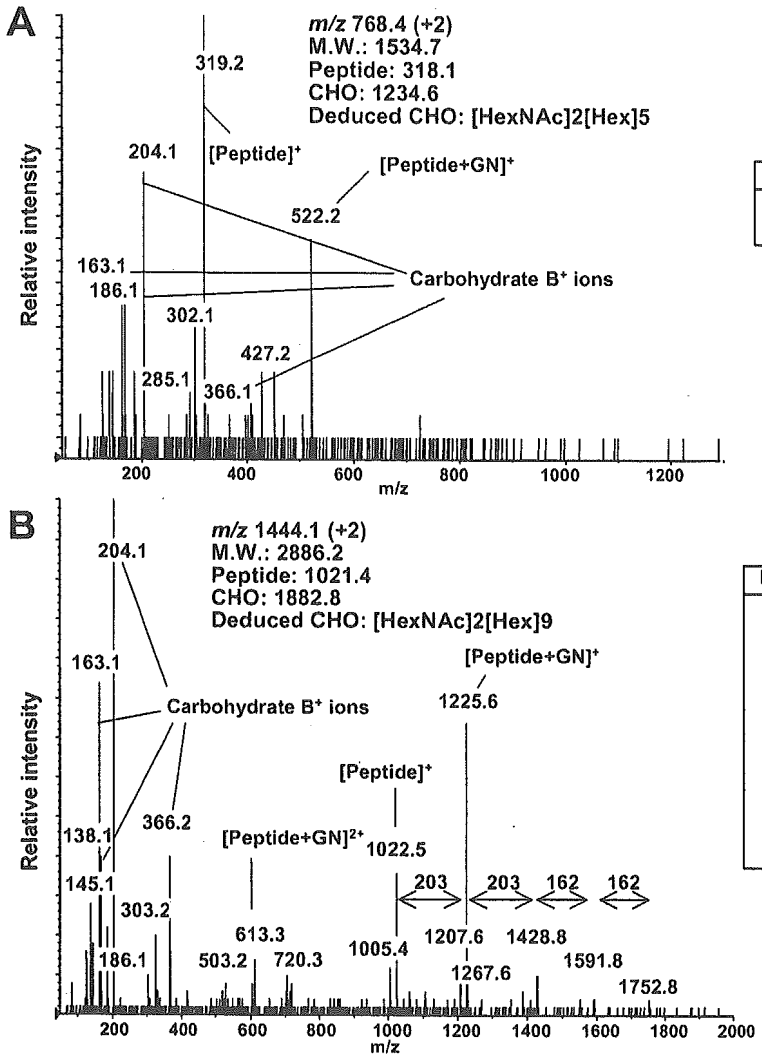

G4

Residue	Mass	b	b-NH3	y	y-NH3
N	114.0	115.1	98.0	319.1	302.1
W	186.1	301.1	284.1	205.1	188.1

G5

Residue	Mass	b	b-NH3	y	y-NH3
S	87.0	88.0	71.0	1022.4	1005.4
G	57.0	145.1	128.0	935.4	918.4
G	57.0	202.1	185.1	878.4	861.3
N	114.0	316.1	299.1	821.3	804.3
T	101.0	417.2	400.1	707.3	690.3
S	87.0	504.2	487.2	606.3	589.2
T	101.0	605.3	588.2	519.2	502.2
D	115.0	720.3	703.3	418.2	401.1
H	137.1	857.3	840.3	303.1	286.1
F	147.1	1004.4	987.4	166.1	149.1

Fig. 6. Product ion spectra of the chymotryptic *N*-glycosylated peptides of apoB100. (**A**) Product ion spectrum of *m/z* 768.4 (+2) at 14 min for the glycopeptide consisting of residues 1341–1342. Peptide b and y ions of the peptide NW were found. Table shows *m/z* of the proposed b- and y-series fragment ions, and the detected ions are underscored. (**B**) Product ion spectrum of *m/z* 1444.1 (+2) at 9 min for the glycopeptide consisting of residues 1347–1356. Several ions are consistent with the b- and y-series fragment ions derived from the peptide SGGNTSTDHF. Table shows *m/z* of the proposed b- and y-series fragment ions, and the detected ions are underscored.

4210, and 4404 (G3, 6, 7, 9–12, and16–19) were predominantly occupied by monosialylated or disialylated biantennary complex type oligosaccharides (Figure 7).

Discussion

Although the role of the carbohydrate structures in LDL and/or apoB100 has been examined in several studies (Attie *et al.*, 1979; Filipovic *et al.*, 1979; Fujioka *et al.*, 2000; Orekhov *et al.*, 1989; Shireman and Fisher, 1979), it is still unknown. It is necessary to elucidate the diversity of the oligosaccharides at each *N*-glycosylation site. This is the first report on the characterization of *N*-linked oligosaccharides in apoB100 at each glycosylation site. The protein was initially carboxymethylated and digested with an enzyme (trypsin or chymotrypsin), and then the complex mixtures of peptides and glycopeptides were subjected to LC/ESI MS/MS analysis. Product ion scan of each precursor ion was carried out in a data-dependent manner. The glycopeptide molecular ions were easily distinguished from peptide ions by the presence of carbohydrate-related oxonium ions, such as *m/z* 204 (HexNAc), 186 (HexNAc–H_2O), 168 (HexNAc–H_2O), 366 (HexHexNAc), and others in product ion spectra. Furthermore, product ion spectra provided information for the elucidation of the amino acid sequence of the glycopeptides.

The oligosaccharide structure could be deduced based on the calculated molecular weight of the oligosaccharide moiety. The glycopeptide precursor ion was assigned using three strageties. (1) By comparing the product ions of the glycopeptide with the expected fragment ions derived from

Table III. Site-specific glycosylation analysis of the chymotryptic digest of apoB100 using LC/ESI MS/MS

			Glycopeptides			Oligosaccharide				
Glycosylation site ID	Retention time (min)	Peptide theoretical MW[a]	*m/z*	Charge	Calculated MW[a]	Calculated MW[a]	Theoretical MW[a]	Relative peak intensity (%)[b]	Composition[c]	Deduced Type[c]
G1	—	560.3	—	—	—	—	—	—	—	—
G2	11	822.3	1344.5	+2	2687.0	1882.7	1882.6	4	[HexNAc]2[Hex]9	High mannose
	11	822.3	1263.5	+2	2525.0	1720.7	1720.6	7	[HexNAc]2[Hex]8	High mannose
	11	822.3	1182.5	+2	2363.0	1558.7	1558.5	15	[HexNAc]2[Hex]7	High mannose
	12	822.3	1101.4	+2	2200.8	1396.5	1396.5	12	[HexNAc]2[Hex]6	High mannose
	12	822.3	1020.4	+2	2038.8	1234.5	1234.4	100	[HexNAc]2[Hex]5	High mannose
G3	12	1088.4	1001.8	+3	3002.4	1932.0	1931.7	70	[HexNAc]4[Hex]5[Neu5Ac]1	Biantennary complex
	15	1088.4	1098.8	+3	3293.4	2223.0	2222.8	100	[HexNAc]4[Hex]5[Neu5Ac]2	Biantennary complex
G4	14	318.1	768.4	+2	1534.8	1234.7	1234.4	—	[HexNAc]2[Hex]5	High mannose
G5	9	1021.4	963.1	+3	2886.3	1882.9	1882.6	100	[HexNAc]2[Hex]9	High mannose
	9	1021.4	1444.1	+2	2886.2	1882.8				
	9	1021.4	1363.1	+2	2724.2	1720.8	1720.6	40	[HexNAc]2[Hex]8	High mannose
	9[d]	1021.4	1282.1	+2	2562.2	1558.8	1558.5	16	[HexNAc]2[Hex]7	High mannose
G6	—	469.2	—	—	—	—	—	—	—	-
G7	—	1023.5	—	—	—	—	—	—	—	-
G8	—	515.3	—	—	—	—	—	—	—	-
G9	—	2846.4	—	—	—	—	—	—	—	-
G10	15	279.1	829.0	+3	2484.1	2223.0	2222.8	—	[HexNAc]4[Hex]5[Neu5Ac]2	Biantennary complex
	15	279.1	1243.0	+2	2484.0	2222.9				
G11	13	521.2	812.7	+3	2435.1	1931.9	1931.7	100	[HexNAc]4[Hex]5[Neu5Ac]1	Biantennary complex
	13	521.2	1218.5	+2	2435.0	1931.8				
	16	521.2	909.8	+3	2726.3	2223.0	2222.8	52	[HexNAc]4[Hex]5[Neu5Ac]2	Biantennary complex
G12	28	878.5	1028.8	+3	3083.4	2222.9	2222.8	—	[HexNAc]4[Hex]5[Neu5Ac]2	Biantennary complex
G13	44	978.5	1341.6	+2	2681.2	1720.7	1720.6	31	[HexNAc]2[Hex]8	High mannose
	44	978.5	1260.6	+2	2519.1	1558.6	1558.5	50	[HexNAc]2[Hex]7	High mannose
	44	978.5	1179.5	+2	2357.1	1396.6	1396.5	100	[HexNAc]2[Hex]6	High mannose